

INVESTIGATIVE NUCLEAR MEDICINE

Positron Tomography with Deoxyglucose for Estimating Local Myocardial Glucose Metabolism

Osman Ratib, Michael E. Phelps, Sung-Cheng Huang, Eberhard Henze, Carl E. Sellin, and Heinrich R. Schelbert

UCLA School of Medicine and the University of California at Los Angeles, Los Angeles, California

The deoxyglucose method originally developed for measurements of the local cerebral metabolic rate for glucose has been investigated in terms of its application to cardiac studies with positron computed tomography (PCT) and fluorodeoxyglucose (FDG). Studies were performed in dogs to measure the tissue kinetics of FDG with PCT and by arterial and venous sampling. The operational equation developed in our laboratory as an extension of the Sokoloff model was used to analyze the data. Error propagation, primarily from corrections applied to remove spillover of activity from the myocardial blood pool to tissue and from partial-volume effects in the PCT images, limited accuracy in the estimation of the individual rate constants for transport, phosphorylation, and dephosphorylation. However, a constant representing the combination of transport and phosphorylation was accurately determined and yielded measured values of the myocardial metabolic rate for glucose (MMRGlc) that were in good agreement with direct determinations using the Fick method over a wide range of glucose metabolic rates (from 1.7 to 21.1 mg/min-100g). The lumped constant (0.67 ± 0.10) was also found accurate and stable over this range of metabolism. The FDG method accurately predicted the true MMRGlc even when the glucose metabolic rate was normal but myocardial blood flow (MBF) was five times the control value, or when metabolism was reduced to 10% of normal and MBF increased to five times normal. Improvements of PCT resolution are required to improve the accuracy of the estimates of the rate constants and the MMRGlc.

J Nucl Med 23: 577-586, 1982

With the recent development of positron computed tomography (PCT), cross-sectional imaging of the heart has become possible (1,2). Such images reflect quantitatively the distribution of radioactive tracer concentrations in myocardium and thus resemble in vivo autoradiograms. This new imaging approach provides a potential nontraumatic means of quantitating regional myocardial metabolism using tracer kinetic models.

Sokoloff et al. (3) recently developed an autoradiographic method and a tracer kinetic model for the

measurement of the local cerebral metabolic rate for glucose using the C-14-labeled glucose analog, 2-deoxyglucose. The 2-deoxyglucose has been labeled with fluorine-18 by Ido et al. (4) to form 2-fluoro-2-deoxy-D-glucose (FDG). FDG has been shown by Bessell et al. (5), Gallagher et al. (6), Reivich et al. (7) and Machado DeDomenech and Sols (8) to be a substrate for hexokinase, with the end product FDG-6-PO₄. Phelps et al. (9) and Huang et al. (10) have shown that the transport and phosphorylation constants for FDG in the human brain are similar to those for DG in the monkey (11), although somewhat lower than values in the rat (3) because of the higher blood flow and metabolic rates in rat brain. Thus, FDG and DG appear to behave similarly as substrates

Received Nov. 11, 1981; revision accepted Feb. 5, 1982.

For reprints contact: Michael E. Phelps, PhD, Div. of Biophysics, Dept. of Radiological Sciences, UCLA School of Medicine, Los Angeles, CA 90024.

competitive with glucose for membrane transport sites and hexokinase.

Because DG-6-PO₄ and FDG-6-PO₄ are not substrates for further metabolism through glycolysis, glycogen formation, or the pentose shunt, and also have low membrane permeability, they accumulate in tissue (3,9,10). The rate of accumulation (or the net accumulation over a given period of time) is proportional to the phosphorylation rate of exogenous glucose. This allows the isolation of the membrane-transport and phosphorylation steps and their mathematical description using the principles of competitive enzyme reactions and tracer kinetics (3,9,10). Studies in dogs, monkeys, and humans by Phelps et al. (12,13) and in rats and dogs by Gallagher et al. (6,14) have shown that FDG is extracted and converted to FDG-6-PO₄ in the myocardium, and suggest that FDG could be used to measure the rate of exogenous glucose utilization in the heart.

In the present study we have investigated the use of FDG, the tracer kinetic model developed in our laboratory (9,10) as an extension of the Sokoloff model (3), and PCT for the determination of the local myocardial rate of glucose metabolism in vivo. These studies in dogs were performed (a) to determine the kinetic constants for transport and phosphorylation of FDG and dephosphorylation of FDG-6-PO₄, (b) to determine the lumped constant, and (c) to examine the stability of the model over a wide range of glucose metabolic rates and in states of severe mismatch between myocardial blood flow and glucose metabolism.

MATERIALS AND METHODS

Preparation of FDG. FDG(F-18) with a specific activity of 10–20 mCi/mg was synthesized by the method developed by Ido et al. (4) as modified by Barrio et al. (15). The radiochemical purity, as assayed by high-pressure liquid chromatography, was >95%.

Animal preparation. Ten mongrel dogs weighing 20–30 kg were anesthetized with sodium pentobarbital (25 mg/kg, i.v.), and small supplemental doses were administered as required. The animals were intubated and ventilated with room air using a Harvard respirator. Catheters were advanced through both femoral arteries into the aorta to monitor systemic blood pressure and withdraw arterial blood for measurements of blood flow with radioactive microspheres. A thoracotomy was performed in the fifth left intercostal space, and the pericardium was incised widely and sutured to the chest wall, forming a cradle in which the heart was suspended. Two polyethylene cannulae were inserted through a puncture wound into the left atrium and used for injection of radiolabeled microspheres and arterial blood sampling. A third catheter was advanced into the coronary sinus to sample myocardial venous blood. ECG and systemic blood pressure, measured through the aortic

catheter with a pressure transducer,* were recorded continuously on a strip-chart recorder.

Two dogs were prepared as described above, but in addition an hydraulic occluder was placed around the left circumflex artery (LCx). Blood flow through the LCx was continuously monitored with an electromagnetic flow probe† placed proximal to the occluder. A 30-gauge needle connected to fine plastic tubing was inserted into the LCx in order to induce coronary hyperemia by a bolus injection of the vasodilator papaverine (1 mg).

Blood samples. Ten millicuries of FDG(F-18) were injected intravenously over a 30-sec interval and arterial and coronary sinus blood samples were obtained. Starting at time zero, samples were withdrawn every 15 sec for 3 min and every minute for the next 12 min. The sampling interval was then progressively lengthened over the next 3 hr. Every sample was divided into two aliquots, one for measurement of FDG activity in whole blood, while the other was immediately placed into an ice bath for measurement of FDG plasma activity and plasma glucose concentrations. FDG activity was measured in a well counter and corrected for radioactive decay ($T_{1/2} = 110$ min). Plasma glucose levels were measured in duplicate by standard enzymatic techniques. Additional arterial and venous samples were taken at the beginning, middle, and end of each experiment for the measurement of free fatty acid and lactic acid concentrations, hematocrit, and blood gases.

Arterial and coronary-sinus plasma activity were used to calculate the myocardial tissue activity curve by the Fick method. The product of A-V difference and plasma flow [plasma flow = whole blood flow \times (1-hematocrit)] was integrated over time. This yielded a myocardial time-activity curve, which was then compared with the tissue curve obtained from the myocardial activity as measured by PCT.

Measurement of myocardial blood flow. Regional myocardial blood flow was determined at the beginning and end of each experiment, using the arterial reference sample technique (16,17) with carbonized polystyrene radioactive microspheres (Co-57 and Sn-113; $15 \pm 3\mu$).

Tomographic imaging. After preparation, each dog was carefully positioned in the UCLA positron computed tomograph (18).‡ A low-power neon laser was used to identify a favorable cross section through the left ventricle. After recording a transmission scan for subsequent correction of photon attenuation, a blood-pool image was acquired for 2 min after in vivo labeling of red blood cells by inhalation of carbon monoxide (0–15). The blood-pool image was used to correct the myocardial F-18 tissue activity for cross contamination from F-18 in the blood pools and the blood activity in myocardial tissue. To allow for sufficient decay of 0–15 ($T_{1/2} = 2.04$ min), FDG was injected 15 min later. Starting at the time of

injection, serial images were recorded at the same level across the heart: an initial set of ten 2-min images was followed by ten 5-min images and by ten 10-min images, resulting in a total scanning time of 3 hr. All image data were collected in the medium-resolution mode with an image resolution of 1.6 cm full width at half maximum. In order to reduce the blurring effect of cardiac motion, the images were gated to the diastolic phase of the cardiac cycle. All images were decay-corrected and normalized to the same acquisition time.

After each experiment the tomograph was calibrated with a cylindrical phantom (20 cm diam) containing a known amount of positron emitter. A known volume (measured with analytical pipets of $\pm 0.5\%$ accuracy) of activity from the calibration phantom was counted in a well counter along with the blood samples of known volume. The ratio of the cpm/cc in the well counter to the cpm/cc of the cylinder in the tomograph provides a calibration factor that relates the tomographic measurement of the myocardial activity to the activity of the blood samples measured in the well counter (9).

After reconstruction of the cross-sectional images, regional myocardial F-18 concentrations were measured as follows. In each experiment, six regions of interest, usually 0.428 cm² large (37 pixels), were assigned to each of the 30 images of the myocardium. A seventh region of interest was placed in the center of the ventricular cavity of the F-18 image for estimation of the FDG blood clearance curve in vivo. Within the regions of interest, the mean counts/pixel were determined. The same regions of interest were also assigned to the CO (O-15) blood-pool image in order to evaluate the amount of contamination from blood activity in each of the myocardial tissue regions. The F-18 tissue data were then corrected for the spillover from blood activity using the relationship

$${}^{18}\text{F}(t)_i = (C^{15}\text{O})_i \frac{{}^{18}\text{F}(t)_{\text{bl}}}{{}^{15}\text{O}(t)_{\text{bl}}}, \quad (1)$$

where $(C^{15}\text{O})_i$ is the O-15 concentration in the myocardial region of interest measured with the PCT. The terms $(C^{15}\text{O})_{\text{bl}}$ and ${}^{18}\text{F}(t)_{\text{bl}}$ are the concentrations in the blood samples as measured in a well counter for a known volume of blood. The terms involving F-18 are determined as a function of time t because the activity concentrations of F-18 in tissue and blood are changing with time. Equation 1 allows the calculation of the local F-18 activity in the image $[{}^{18}\text{F}(t)_i]$ of the myocardium, due to spillover of activity from blood chambers and that due to activity in the vascular space of the myocardium itself. These values were calculated for each region of interest and were subtracted from the corresponding tissue F-18 concentration to allow the determination of the interstitial FDG plus FDG-6-PO₄ concentrations.

A second correction was needed because of the partial-volume effect related to object size (19), which

causes an underestimation of the tracer concentrations on the PCT images if the size of the object is close to or smaller than the resolution of the tomograph. The recovery coefficients (RC) used to correct for this partial-volume effect have been established initially in phantom studies by Hoffman et al. (19), and their use for in vivo measurements was subsequently confirmed by Wisenberg et al. (20). The RC is the apparent tracer concentration in the image divided by the true tracer concentration; it is unity for large objects in which there are no significant partial-volume effects.

These corrections require knowledge of the myocardial wall thickness, which was determined in vivo by echocardiography and also postmortem as follows. At the end of each experiment, the plane of the cross-sectional image was identified on the heart with the aid of the low-power neon laser and was carefully marked on the surface of the left ventricle. The dog was then killed with concentrated KCl, the heart was removed, and a thick slice (1.6 cm) taken at the level of the PCT image. The shape of this slice was then drawn on a 1 to 1 scale. The wall thickness was measured at the location of each region of interest on the images, and the data divided by the corresponding recovery coefficient (19).

Calculation of the rate constants, lumped constant, and glucose metabolic rate. As demonstrated previously for the brain (7,9,10), the myocardial metabolic rate of glucose (MMRGlc) from exogenous sources can be derived from the kinetics of FDG using an extension of the Sokoloff model (3) by Phelps and Huang (9,10). This model assumes three compartments: a plasma compartment, a tissue compartment for glucose and FDG, and a tissue compartment for phosphorylation of glucose and FDG to glucose-6-PO₄ and FDG-6-PO₄ (Fig. 1). These are referred to as Compartments 1, 2, and 3. The boundary between Compartments 1 and 2 consists of the capillary and cell membranes. Compartments 2 and 3 are not separated by a physical barrier but they are by the phosphorylation reaction catalyzed by hexokinase, and dephosphorylation by phosphatase. Thus, the capillary and cell membranes are lumped together in the form of the operational model equation of Sokoloff et al. (3) and Phelps and Huang et al. (9,10).

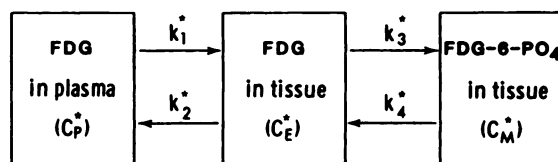


DIAGRAM OF THE THREE COMPARTMENTS IN FDG MODEL

FIG. 1 Scheme of compartmental tracer kinetic model for FDG. Terms C_p^* , C_e^* , and C_m^* are, respectively, concentrations of FDG in plasma and in tissue, and of FDG-6-PO₄ in tissue. The k^* s are the rate constants for forward and reverse membrane transport (endothelium and cell), hexokinase-mediated phosphorylation, and phosphatase-mediated dephosphorylation.

In this model, if FDG-6-PO₄ is trapped in Compartment 3, its concentration is directly related to MMRGlc. The terms k_1^* to k_4^* (Fig. 1) are first-order rate constants that can be determined using the operational equation of the model (9,10) if the rates of change for total tissue F-18, plasma FDG, and plasma glucose concentration are known as a function of time. The time-dependent F-18 tissue concentration curves were obtained by two methods: by PCT imaging and by blood sampling to determine the arterio-venous FDG difference across the heart as a function of time (see Fig. 8). These values are then used to calculate the four values of the k_s^* by a least-squares estimation routine. The operational equations of the model and description of the analysis are given elsewhere (9,10).

Assuming k_4^* to be small [i.e., low enzyme activity of the phosphatase that hydrolyzes FDG-6-PO₄, (21)] and with knowledge of the specific rate constants of the model, one can calculate the metabolic rate of glucose according to the formula (9,10)

$$\text{MMRGlc} = \frac{[\text{Glc}]}{\text{LC}} k_3^* k_1^* / (k_2^* + k_3^*), \quad (2)$$

where [Glc] is the capillary plasma glucose concentration and LC is the lumped constant that accounts for difference in transport and phosphorylation between FDG and glucose (3,9,10). The term $k_3^* k_1^* / (k_2^* + k_3^*)$, which describes the combination of transport and phosphorylation of FDG, will be replaced by a single constant K^* . The value of LC has been shown (9,10) to be

$$\text{LC} = \frac{[\text{Glc}] k_3^* k_1^* / (k_2^* + k_3^*)}{\text{MR}_f}, \quad (3)$$

where MR_f is the metabolic rate of exogenous glucose measured according to the Fick principle:

$$\text{MR}_f = \text{MBF}(A - V), \quad (4)$$

where MBF is the myocardial blood flow and A and V

are arterial and venous plasma concentrations of glucose across the heart.

Uncoupling of flow and metabolism. The independence of the FDG model from myocardial blood flow (MBF) was examined in the following manner. Papaverine (1 mg) was injected into the left circumflex artery to produce an increase in MBF without producing a significant change in metabolism (22). This resulted in high local MBF with normal local metabolism in the distribution of the artery. During this state, ¹³NH₃ and labeled microspheres were injected into the left atrium; 5 min were allowed for equilibration of ¹³NH₃, and a PCT image of the myocardium was recorded. After 70 min, the papaverine administration was repeated, FDG (5 mCi) was injected intravenously, and microspheres were injected into the left atrium. PCT and blood sampling were performed to estimate the rate constants and MMRGlc as described above.

This same sequence was repeated except that hyperemia was induced by occluding the LCx for 30 min and then releasing the occluder to produce reactive hyperemia. At the peak of the hyperemic MBF response (determined with the electromagnetic flow probe), FDG and labeled microspheres were injected intravenously and into the left atrium, respectively. The reactive hyperemia after a 30-min total occlusion produces a state of high MBF and low glucose metabolism (about 30–50% of control values for 10–20 min) due to residual tissue acidosis (23). The MMRGlc was calculated using the directly measured rate constants and Eq. (2).

RESULTS

A typical example of a kinetic study is shown in Fig. 2. Sixteen out of 30 serial images obtained at the same cross-sectional level over a 200-min period after injection are shown at the left of the figure. The kinetic tissue data to the right were obtained from six regions of interest in the left ventricle. The counts in these regions were av-

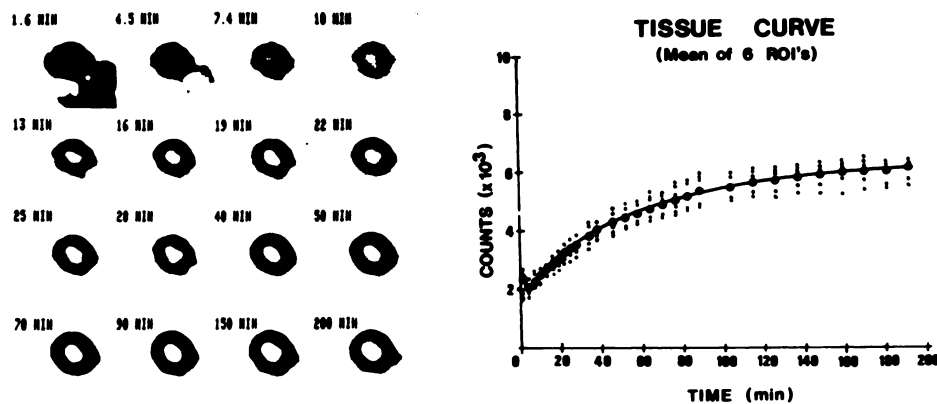


FIG. 2. Left: Example of series of tomographic images as a function of time for a single cross section through the heart after i.v. injection of FDG. Examples are shown for 16 time intervals out of the total 30. Right: Numerical data from this kinetic study, showing individual kinetic curves for six different regions (points) and also mean value for total number of regions of interest (solid line).

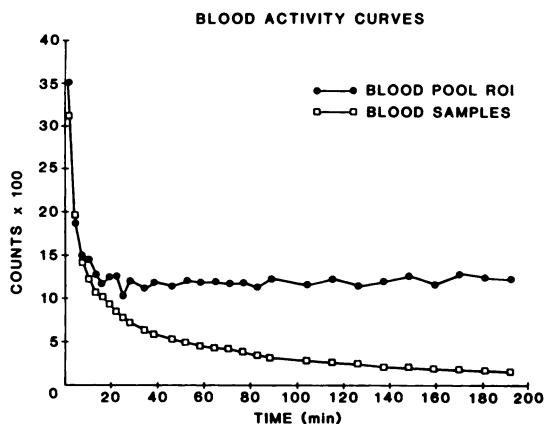


FIG. 3. Example of FDG blood curves comparing samples counted externally and measured in vivo with PCT.

eraged and the best fit by least-squares analysis was plotted. The initial part of the curve, corresponding to the early images where blood activity is high and myocardial activity low, is dominated by blood-pool activity. Correction for this contamination was performed in all experiments using the spillover correction shown in Eq. (1). Blood activity could not be measured directly from the images because of a reverse movement of myocardial activity into the blood in the cardiac chambers. The activity measured in the center of the ventricular cavity agreed with the value obtained from arterial blood samples only at the very early times, when there was a high ratio of blood-to-myocardial activity (Fig. 3).

The spillover fraction—measured on the blood-pool image by taking the ratio of activity in each region of interest to activity in the center of the ventricle—averaged 0.36 ± 0.12 s.d., ranging from 0.19 to 0.56 for values throughout the myocardial sections and for all dog

experiments. The portion of this fraction due to activity contained in tissue blood is expected to be about 10% (unpublished data).

The data of each region of interest were further corrected for a partial volume using the recovery coefficient determined in phantom studies (19) and corresponding to the thickness of the myocardium. The effects of the two corrections are shown in Fig. 4. The correction for blood-pool spillover, shown in the center, resulted in a more realistic curve of early myocardial tissue uptake of FDG. The right-hand panel shows the same data after correction for the partial-volume effect. This correction significantly reduced the scatter in the values from different regions of interest. The mean curve shows a higher total tissue uptake than in the left-hand panel, indicating that without the partial-volume correction the uptake rate and total tissue radioactivity concentration were underestimated. This, of course, results in an underestimation of the MMRGlc; only the metabolic rate obtained from the corrected curve was in agreement with the metabolic rate obtained by the Fick method.

The effect of the spillover of activity from the chamber to the myocardium was also greatest when the MMRGlc was low, as is illustrated in the studies of Figs. 5 and 6, where the values of the MMRGlc were 5.08 and 19.9 mg/min-100 g, respectively. This results from the fact that, as MMRGlc increases, the rate of formation and total amount of the FDG-6-PO₄ also increases compared with the surrounding activity, as is apparent in the images and numerically in the curves of Figs. 5 and 6.

Blood activity of FDG. FDG clears rapidly from the arterial and coronary-sinus blood, as shown in Fig. 7. The expanded early portion of the curve (left) shows the time difference between the arterial and the venous peaks of

MEAN TISSUE CURVE

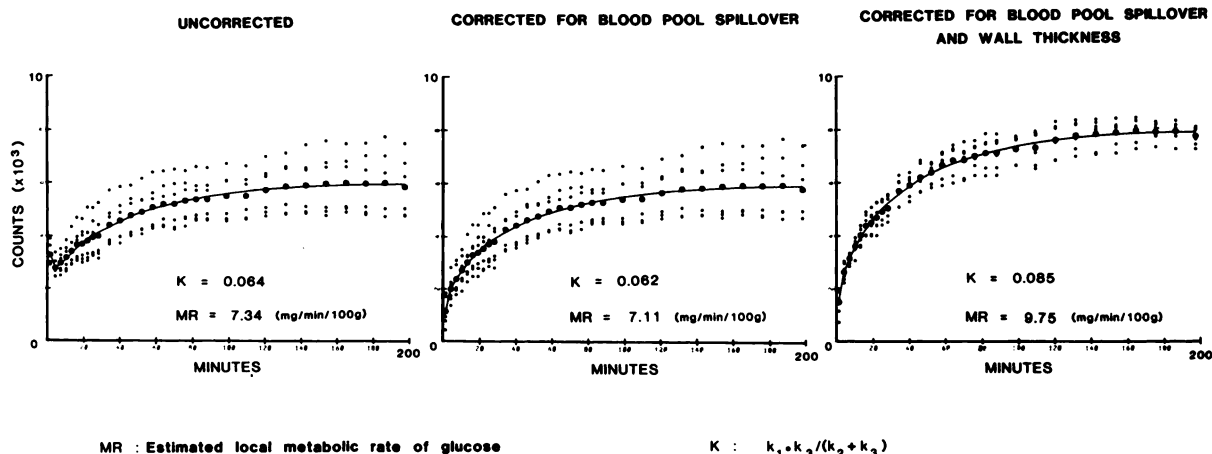


FIG. 4. Example of tissue kinetic curves showing effect of correcting for blood-pool spillover of activity into myocardium, and for partial-volume effect. Points are from individual regions of interest, and solid line is mean value for them. Note that correction for spillover is most dramatic at early portions of tissue uptake curve. Partial-volume correction elevates entire curve, and also has most dramatic effect on calculated metabolic rate (MR).

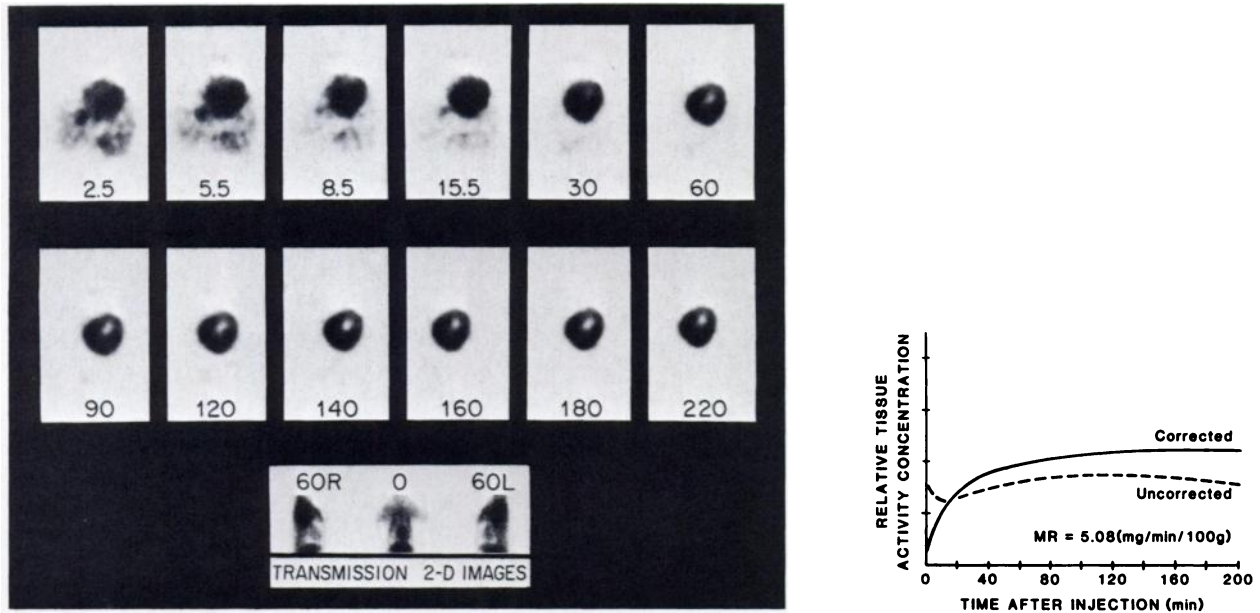


FIG. 5. (A) Selected series of tomographic images taken after i.v. injection of FDG in animal with low glucose metabolic rate. Note that until ~30 min myocardium differs little from surrounding activity and that in blood pool of cardiac chambers (cf. Fig. 6). Numbers below images show minutes after injection. In transmission images (below), "0" indicates conventional A-P view, flanked by right and left obliques; these were used to align dog for PCT study. (B) Kinetic data from this study show impact of spillover and partial-volume correction when metabolic rate of glucose is low.

activity. This delay averaged 0.24 ± 0.04 min, and represents the combination of blood transit time across the heart and the rapid forward and reverse exchange between blood and interstitial space due to the changes with time after injection in the blood-to-tissue concentration gradient.

Metabolic rate and lumped constant (LC). The tissue

curves obtained from the images were used to estimate k_1^* to k_4^* of the FDG compartmental model (9,10). Because of the proportionately high values of the corrections applied to the data and the propagation of errors through these corrections (i.e., limitations imposed by the present PCT resolution), the true value of each k^* could not be satisfactorily estimated. However, the es-

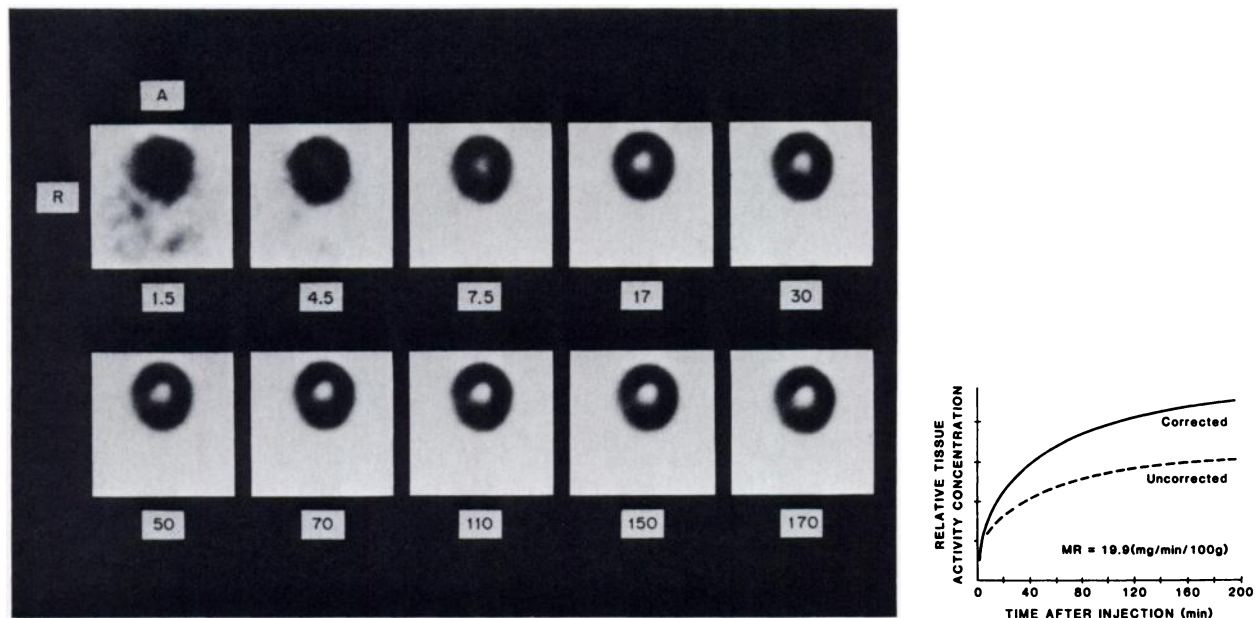


FIG. 6. (A) Successive tomographic images as a function of time after i.v. injection of FDG when glucose metabolic rate is high. Note earlier delineation of myocardium from adjacent areas, due to rapid sequestering of FDG-6- PO_4 in myocardium. Minutes after injection are shown below. These 10 scans shown have been selected from 40 images taken during 3 hr. (B) Kinetic data show impact of blood-pool spillover and partial-volume correction when metabolic rate is high. Here spillover correction at early stages is less important (cf. Fig. 5B).

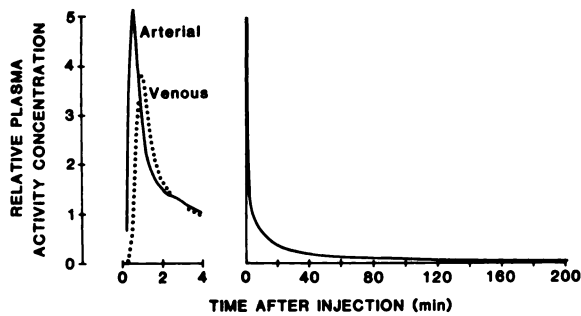


FIG. 7. Left: Arterial and coronary-sinus time-activity curves across the heart after i.v. injection of FDG. Note rapid clearance from plasma. Time displacement and difference in magnitude are due to (a) transit across the heart, (b) forward and reverse diffusion of FDG from plasma and tissue, and (c) fraction of FDG that is phosphorylated and remains in heart. Right: clearance curve for arterial plasma.

estimate of the combined rate constant K^* , which is the product of the rate constants of phosphorylation, k_3^* , and the distribution volume of FDG $[k_1^*/(k_2^* + k_3^*)]$, was found to be reliable and had minimum variability introduced by errors generated in the corrections. The constant K^* is the fractional utilization constant, i.e., the rate constant describing the fractional rate at which plasma FDG is transported across the capillary and cell membranes and then phosphorylated. This constant was then used to calculate the lumped constant, LC, in each experiment according to Eq. (3). The results obtained are listed in Table 1. The same calculation was applied to the tissue curves obtained from arterio-venous (A-V) difference in plasma FDG. Figure 8 shows a comparison of the kinetic curves obtained from the same animal by PCT and A-V sampling. It demonstrates that the tomograph is providing good estimates of the absolute tissue activity concentrations, as has been directly vali-

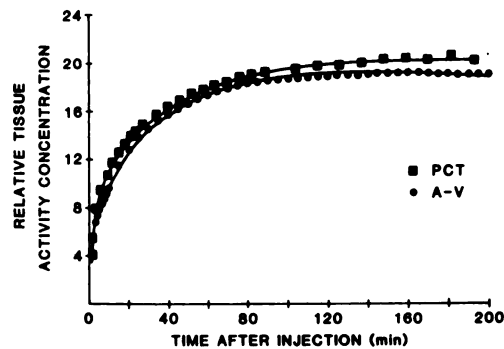


FIG. 8. Comparison of myocardial tissue uptake curves generated (a) by time integration of arterio-venous FDG difference across the heart (see method section), and (b) recorded in vivo with PCT. FDG was injected intravenously.

dated previously for this same system and animal model (20). Differences will exist between these two measurements because the A-V difference samples the whole heart and PCT samples only one cross section. In addition, there are measurement errors in both techniques.

The mean value of 0.68 ± 0.1 for LC was used to recalculate the exogenous metabolic rate using Eq. (2) for each individual experiment. The metabolic rate calculated in this manner was compared with the metabolic rate of glucose determined by the Fick method. The excellent agreement between the two measurements is shown in Fig. 9A. Because the dietary state of the dogs was not controlled, a wide range of myocardial glucose metabolic rates was observed, ranging from 1.7 to 21.1 mg of glucose/min-100 g of tissue. This reflects the capability of the myocardium to utilize alternative substrates, such as free fatty acids and lactic acid, to meet its energy requirements.

The MMRGlc was also calculated from both the PCT

TABLE 1. DATA OF CALCULATED VALUES OF THE FRACTIONAL UTILIZATION CONSTANT (K^*) AND LUMPED CONSTANT (LC) DETERMINED BY PCT AND ARTERIAL-VENOUS SAMPLING METHODS.[†]

Dog	K^*		LC		MR FICK (mg/min/100 g)
	(PCT)	(A-V)	(PCT)	(A-V)	
28	0.035	0.029	0.67	0.56	5.31
29	0.081	0.062	0.68	0.56	12.98
30	0.100	0.088	0.76	0.67	11.95
31	0.098	0.122	0.56	0.70	21.20
32	0.020	—	0.89	—	1.70
35	0.099	0.082	0.70	0.58	16.9
36	0.029	—	0.58	—	4.97
37	0.028	0.022	0.77	0.62	5.08
38	0.113	0.131	0.58	0.64	19.90
39	0.074	0.101	0.61	0.84	13.60
Mean	0.067	0.080	0.68	0.66	11.36
S.D.	± 0.036	± 0.039	± 0.10	± 0.09	± 6.82

[†] Values are shown for different glucose metabolic rates (MR) as determined by the Fick method.

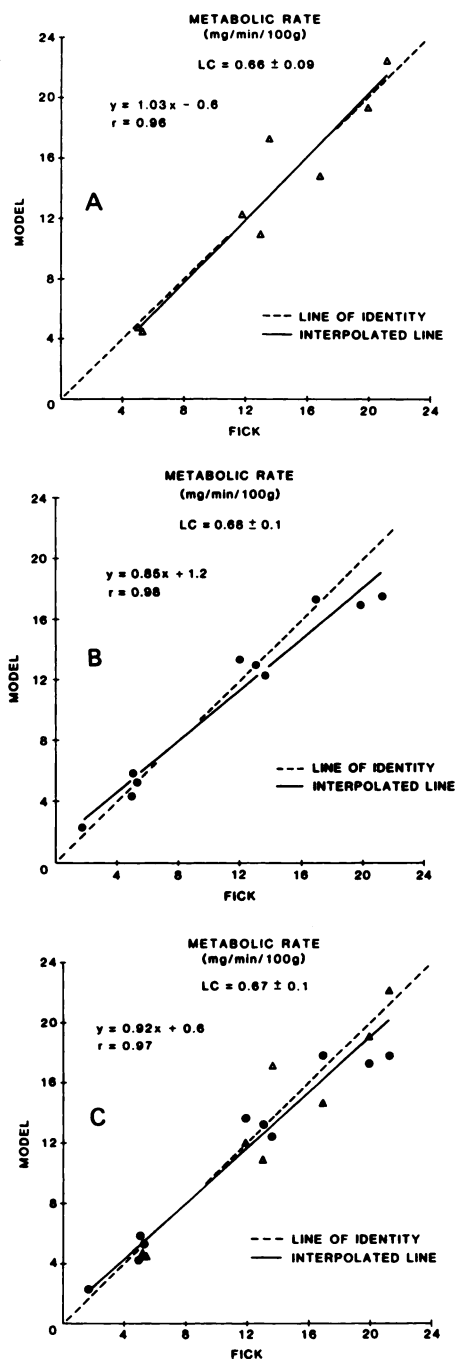


FIG. 9. (A) Plot showing correlation between glucose metabolic rate as calculated from Fick method and that from FDG model with rate constants generated from tissue uptake curve using arterial and venous measurements of FDG. (B) Same as (A) except that rate constants and glucose metabolic rate calculated with FDG were determined with PCT. (C) Combined data of (A) and (B). There was no statistically significant difference between the fits in (A), (B), and (C), indicating the good correlation between in vivo PCT estimates of metabolic rate and direct sampling techniques.

and A-V kinetic FDG data using Eq. (2). These values were correlated with the estimates from the Fick method individually (Figs. 9A, 9B) and in a combination (Fig. 9C). Although each of these correlations shows a

somewhat different slope and intercept, there was no statistically significant difference. Thus, the PCT estimates agreed very well with the measurements by the direct A-V sampling approach for FDG and by the Fick method.

To assess the stability of myocardial glucose metabolism during the time period of the study, we determined the variability of the myocardial arterio-venous glucose difference as a function of time. From time of FDG injection to the end of the experiment, the A-V values exhibited an average standard deviation of $\pm 8\%$. The variation in the average microsphere-estimated MBF, taken at the start and end of each experiment, was $\pm 9\%$. The stability of the A-V glucose and MBF indicates that the myocardial metabolic rate for exogenous glucose was relatively constant during the time course of each study.

Uncoupling of metabolism from blood flow. An example of the measurement of MMRGlc when glucose metabolism and MBF are uncoupled is shown in Fig. 10. The $^{13}\text{NH}_3$ image shows the papaverine-induced hyperemia (MBF = 490 ml/min-100 g as measured with microspheres) in the LCx distribution (arrow) relative to the normal MBF (86 ml/min-100 g) in the remainder of the cross section (24). The MMRGlc image with FDG under the same papaverine-induced hyperemia shows the uniform and correct distribution of glucose metabolism throughout the left ventricle, even though the MBF in LCx distribution is about five times that of the rest of the myocardium. Although the smooth-muscle relaxant papaverine has a positive inotropic effect—and hence can alter myocardial metabolism—this effect appears to be small in relation to the tremendous hyperemic response. Furthermore, as indicated by studies in isolated dog myocardium, a bolus administration of only 3 μmole of papaverine would have only a minimal effect on myocardial metabolism (22).

The far right-hand image in Fig. 10 shows the reduced

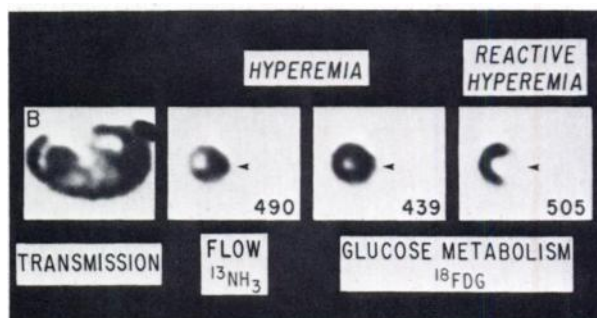


FIG. 10. Study illustrating the independence of the FDG method from blood flow. At left is transmission scan showing cross section of opened chest (B). Numbers below PCT images are flow rates in ml/min-100 g in left circumflex distribution (arrows) as determined by microspheres. Flow in rest of LV was 85–90 ml/min-100 g in each experiment. Anterior is at left of image and left side of cross section is at bottom of image.

glucose metabolism in the LCx segment resulting from occluding the LCx for 30 min and then releasing the occluder to produce reactive hyperemia. At the time of reperfusion, reactive hyperemia in the tissue supplied by the LCx occurs, whereas return of glycolysis to control levels is delayed because of the residual tissue acidosis (23). The calculated MMRGlc in the LCx distribution was about 19% of the value in the remainder of the normal tissue. Mochizuki and Neely (23) found that 30 min of ischemia in the rat heart reduced exogenous glucose utilization to 30% of control, with a very slow recovery over the 30 min of reperfusion. Thus, in this latter case, the FDG method estimates the reduced MMRGlc even though there is a large MBF/MMRGlc mismatch (i.e., MBF is increased 5.6 times and glucose metabolism is reduced to $\sim 1/5$ relative to control values). The serial PCT images showed high F-18 activity in the LCx segment initially, reflecting the high MBF and transport into tissue. However, the tissue activity rapidly decreased as the high MBF removed FDG from the tissue and only small amounts of FDG were phosphorylated because of the low glucose metabolic rate in the LCx distribution.

DISCUSSION

As shown in Table 1, the LC estimated in each experiment did not vary significantly over a wide range of metabolic rates. Thus the evaluation of local myocardial MMRGlc is feasible using a mean value of LC in the model. The calculated MMRGlc from the FDG model showed a good correlation with the value obtained by the Fick method (Fig. 9). This indicates the reliability of the model in the evaluation of MMRGlc over a wide range of metabolic states.

The value of LC found in this work (0.67 ± 0.10) is higher than those reported for the brain with DG: 0.483 in the rat (3), 0.344 in the monkey (11), or 0.420 with FDG in man (9,10). However, studies also performed in our laboratory (unpublished data) using the isolated perfused rabbit myocardium have yielded a value of 0.60 ± 0.10 (s.d.) for FDG, which is in good agreement with the value reported here.

Estimation of the plasma input function by in vivo measurements of blood activity in the cardiac chambers with PCT requires good tomographic resolution and cardiac gating. At late times after injection of FDG, the spillover from activity in myocardium to the cardiac chambers produces a significant overestimation of the blood activity concentration.

The studies in which MBF and metabolism were uncoupled by large local increases in MBF with normal or severely reduced MMRGlc (Fig. 10) illustrate the viability of the model under these demanding conditions. The results provide experimental confirmation of the

postulated low sensitivity of the model to changes in blood flow (3,9,10).

In this work, the values of the rate constants for transport, phosphorylation, and dephosphorylation were estimated from the time course of the plasma FDG concentration and the myocardial F-18 tissue concentration with PCT or with the A-V sampling technique for measuring the temporal sequence of FDG tissue uptake. The values of the rate constants k_1^* , k_2^* , k_3^* , and k_4^* —estimated from both sets of data using least-squares curve fitting to the FDG model—produced comparable results. Reasonable convergence was usually achieved within 20 iterations. In some studies we experienced a slower convergence and greater difficulty in obtaining acceptable values for the individual rate constants. However, the value of the factor $k_1^* k_3^*/(k_2^* + k_3^*)$ was found to be remarkably insensitive to the exact fitting results. In other words, the value of this factor converges rapidly and is quite insensitive to the initial values chosen for the curve fitting. This allowed accurate estimates of local MMRGlc to be determined, even though estimates of the individual constants were found unsatisfactory.

The large variation in the values of the individual rate constants is to be expected in this study with such large variations in MMRGlc (i.e., 1.7–21.1 mg/min-100 g) but the numerous correction factors used produced uncertainties in the data that added inaccuracies to the estimates of the individual constants. This was most prominent in the fitting of the early part of the tissue curves (i.e., the first 25 min) when F-18 uptake in tissue increases most rapidly. Also, the early part of the tissue curve is most sensitive to errors in the corrections applied to the data for the contamination of the tissue data from blood-pool activity. The correction for the underestimation of tissue activity due to a partial-volume effect was performed by multiplying the data by recovery coefficients that ranged from 1.6 to 2.5. Thus, these corrections were large enough so that inaccuracies in their values would produce significant errors.

The validity of these corrections, however, can be assessed in two ways: First, only the MMRGlc obtained from the corrected curves showed a good correlation with the MMRGlc obtained using the Fick method (Fig. 9). Second, in all our experiments the corrected tissue curve determined with PCT matched the tissue curve obtained by integrating the A-V difference for FDG in plasma, as shown in a typical case in Fig. 8. The uncorrected tissue curve systematically underestimated the total activity in tissue, owing to the partial-volume effect and a slow rate of increase at the early times due to contamination from blood activity.

These corrections are directly related to the spatial resolution of the tomograph. An improvement in resolution will significantly reduce their magnitude and provide more reliable estimates of the individual rate constants.

FOOTNOTES

- * Statham P23 Db.
- † Series 500, Biotronix.
- ‡ ECAT 18, EG&G Ortec, Inc., Oak Ridge, TN.

ACKNOWLEDGMENTS

This work was supported in part by DOE contract No. DE-AM06-76-SF00012 and by the Swiss National Foundation of Research (Dr. Ratib).

REFERENCES

1. PHELPS ME, HOFFMAN EJ, MULLANI NA, et al: Application of annihilation coincidence detection to transaxial reconstruction tomography. *J Nucl Med* 16:210-223, 1975
2. PHELPS ME: Emission computed tomography. *Semin Nucl Med* 7:337-365, 1977
3. SOKOLOFF L, REIVICH M, KENNEDY C, et al: The [¹⁴C] deoxyglucose method for the measurement of local cerebral glucose utilization: Theory, procedure, and normal values in the conscious and anesthetized albino rat. *J Neurochem* 28: 897-916, 1977
4. IDO T, WAN WN, CASELLA V, et al: Labeled 2-deoxy-D-glucose analogs. ¹⁸F-labeled 2-deoxy-2-fluoro-D-glucose, 2-deoxy-2-fluoro-D-mannose, and ¹⁴C-2-deoxy-2-fluoro-D-glucose. *J Label Compd Radiopharm* 14:174-183, 1978
5. BESSELL EM, FOSTER AB, WESTWOOD JH: The use of deoxyfluoro-D-glucopyranoses and related compounds in a study of yeast hexokinase specificity. *Biochem J* 128:199-204, 1972
6. GALLAGHER BM, ANSARI A, ATKINS H, et al: Radiopharmaceuticals XXVII. ¹⁸F-labeled 2-deoxy-2-fluoro-D-glucose as a radiopharmaceutical for measuring regional myocardial glucose metabolism in vivo: Tissue distribution and imaging studies in animals. *J Nucl Med* 18:990-996, 1977
7. REIVICH M, KUHL D, WOLF A, et al: The (¹⁸F) fluoro-deoxyglucose method for the measurement of local cerebral glucose utilization in man. *Circ Res* 44:127-137, 1979
8. MACHADO DeDOMENECH EE, SOLS A: Specificity of hexokinases towards some uncommon substrates and inhibitors. *FEBS Lett* 119:174-176, 1980
9. PHELPS ME, HUANG SC, HOFFMAN EJ, et al: Tomographic measurement of local cerebral glucose metabolic rate in humans with (¹⁸F)2-fluoro-2-deoxy-D-glucose: Validation of method. *Ann Neurol* 6:371-388, 1979
10. HUANG SC, PHELPS ME, HOFFMAN EJ, et al: Noninvasive determination of local cerebral metabolic rate of glucose in man. *Am J Physiol* 238:E69-E82, 1980
11. KENNEDY C, SAKURADA O, SHINOHARA M, et al: Local cerebral glucose utilization in the normal conscious macaque monkey. *Ann Neurol* 4:293-301, 1978
12. PHELPS ME, HOFFMAN EJ, SELIN C, et al: Investigation of [¹⁸F]2-fluoro-2-deoxyglucose for the measurement of myocardial glucose metabolism. *J Nucl Med* 19:1311-1319, 1978
13. PHELPS ME, SCHELBERT HR, HOFFMAN EJ, et al: Physiologic tomography studies of myocardial glucose metabolism, perfusion and blood pools with multiple gated acquisition. *Adv Clin Cardiol* 1:373-393, 1980
14. GALLAGHER BM, FOWLER JS, GUTTERSON NI, et al: Metabolic trapping as a principle of radiopharmaceutical design: Some factors responsible for the biodistribution of [¹⁸F]2-deoxy-2-fluoro-D-glucose. *J Nucl Med* 19:1154-1161, 1978
15. BARRIO JR, MACDONALD NS, ROBINSON GD JR, et al: Remote, semiautomated production of F-18-labeled 2-deoxy-2-fluoro-D-glucose. *J Nucl Med* 22:372-375, 1981
16. HEYMANN MA, PAYNE BD, HOFFMAN JIE, et al: Blood flow measurements with radionuclide-labeled particles. *Prog Cardiovasc Dis* 20:55-79, 1977
17. SCHELBERT HR, PHELPS ME, HOFFMAN EJ, et al: Regional myocardial perfusion assessed with N-13 labeled ammonia and positron emission computerized axial tomography. *Am J Cardiol* 43:209-218, 1979
18. PHELPS ME, HOFFMAN EJ, HUANG SC, et al: ECAT: A new computerized tomographic imaging system for positron-emitting radiopharmaceuticals. *J Nucl Med* 19:635-647, 1978
19. HOFFMAN EJ, HUANG SC, PHELPS ME: Quantitation in positron emission computed tomography. I. Effect of object size. *J Comput Assist Tomogr* 3:299-308, 1979
20. WISENBERG G, SCHELBERT HR, HOFFMAN EJ, et al: In vivo quantitation of regional myocardial blood flow by positron-emission computed tomography. *Circulation* 63: 1248-1258, 1981
21. ANCHORS JM, HAGGERTY DF, KARNOVSKY ML: Cerebral glucose-6-phosphatase and the movement of 2-deoxy-D-glucose across cell membranes. *J Biol Chem* 252:7035-7041, 1977
22. ENDOH M, HONMA M: Effects of papaverine and its interaction with isoprenaline and carbachol on the contractile force and cyclic nucleotide levels of the canine ventricular myocardium. *Naunyn-Schmiedeberg Arch Pharmacol* 306: 241-248, 1979
23. MOCHIZUKI S, NEELY JR: Energy metabolism during reperfusion following ischemia. *J Physiol (Paris)* 76:805-812, 1980
24. SCHELBERT HR, PHELPS ME, HOFFMAN EJ, et al: Regional myocardial perfusion assessed with N-13 labeled ammonia and positron emission computerized axial tomography. *Am J Cardiol* 43:209-218, 1979

Specialty Certifying Examination in Nuclear Medicine

The American Board of Nuclear Medicine announces that the examination for certification in the specialty of nuclear medicine will be given September 11, 1982.

Application forms and information concerning certification may be obtained from the American Board of Nuclear Medicine, Inc., 900 Veteran Ave., Los Angeles, CA 90024.